AUV Motion-Planning for Photogrammetric Reconstruction of Marine Archaeological Sites

Vaibhav K. Viswanathan, Zayra Lobo, Jessica Lupanow, Sebastian Seibert von Fock, Zoë Wood, Timmy Gambin, and Christopher Clark

***Abstract*— This paper presents a method for constructing 3D maps of marine archaeological sites using deployments of Autonomous Underwater Vehicles (AUV) equipped with sonar and cameras. The method requires multiple AUV missions in which the first mission directs the AUV to conduct a high altitude lawnmower scan over the area to create a course bathymetry map using sonar. Subsequent AUV missions then direct the AUV to make low altitude fly-overs just above the wreck with the goal of obtaining camera images from multiple viewpoints of the wreck to enable offboard 3D mapping via photogrammetric reconstruction. This approach uses a coarse map generated after the first mission to construct AUV paths that attempt to maximize information gain, i.e. maximize the number of viewpoints of the wreck within a time limit. Presented is a motion planner derived from Rapidly-Exploring Random Trees (RRT) that have sampling strategies modified for this problem. Specifically, the random node selection and new node generation are designed to consider the kinematics of an AUV and the information gain associated with each flyover. Simulation results demonstrate improvements of up to 152% when these sampling strategies are used. Experiment results, involving deployments for mapping two known wrecks located along the coast of Malta, validate the system's ability to construct 3D maps and associated visualizations.**

I. INTRODUCTION

A major challenge marine archaeologists face is the search for and study of marine archaeological sites. They utilize tools such as towed side scan sonar and, more recently, Autonomous Underwater Vehicles (AUVs) equipped with sonars to locate these sites. Once a site is found, it is typically investigated via divers for shallow water ($< 100m$) excavations or working class Remotely Operated Vehicles (ROVs) for deeper waters.

Recently, both divers and ROVs have been equipped with HD cameras to obtain image data suitable for constructing high-resolution (0.01m) 3D maps of wrecks. Fig. 1(a) presents one example: a visualization of a 3D map of a Bristol Beaufighter plane wreck found off the coast of Malta.

V. Viswanathan, Z. Lobo, and J. Lupanow are with the Department of Engineering, Harvey Mudd College, Claremont, CA 91711, USA vviswanathan@hmc.edu, zlobo@hmc.edu, jlupanow@hmc.edu

S. Seibert von Fock is with the Department of Computer Science, California Polytechnic State University, San Luis Obispo, CA 93405, USA sseibertvonfock@gmail.com

Z. Wood is with the Faculty of Computer Science, California Polytechnic State University, San Luis Obispo, CA 93405, USA zwood@csc.calpoly.edu

T. Gambin is with the Faculty of Department of Classics and Archaeology, University of Malta, Msida, Malta timmy.gambin@um.edu.mt

C. Clark is with the Faculty of Engineering, Harvey Mudd College, Claremont, CA 91711, USA clark@hmc.edu

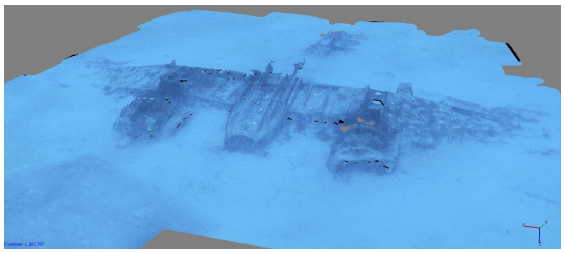

(a)

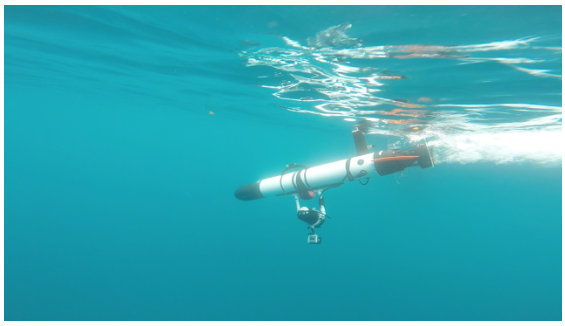

(b)

Fig. 1: (a) A 3D reconstruction of a Bristol Beaufighter made with data collected by divers. (b) The OceanServer Iver2 AUV with BlueView Multibeam Sonar and GoPro Hero 2.

To eliminate the need for divers excavating wrecks in deep, dangerous environments or expensive ROVs, we propose to use AUVs deployed from small boats or the shore, thereby also eliminating the need for expensive ship time. The AUVs are to be equipped with sonar and video camera (Fig. 1b), each used for different mission deployments of a mapping expedition.

This paper presents a method for AUV mapping of wrecks, including a sampling based planner for generating the AUV paths. Specifically, our contributions include:

- An AUV based method for mapping underwater archaeological sites that requires reduced infrastructure (e.g. no underwater positioning system or ship time).
- A sampling based planner with modified node selection and edge expansion steps that demonstrate two orders of magnitude of performance gain when constructing AUV paths to maximize information gain.
- Successful AUV deployments in the coastal region of Malta dedicated to mapping two particular wrecks. 3D visualizations of wreck maps were constructed.

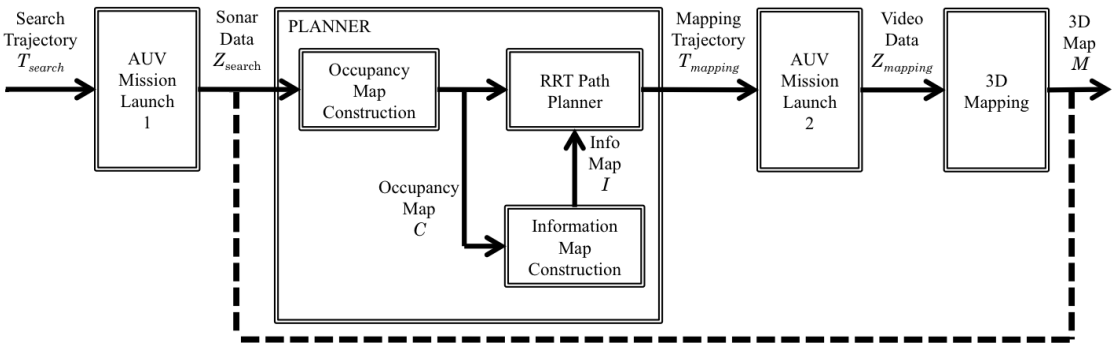

Fig. 2: Block diagram of high-level steps of data collection

This paper is organized as follows. Section II describes related research in the area of motion planning, underwater robots, and their application to archaeological work. Section III outlines the proposed shipwreck mapping methodology, including a description of the sampling based motion planner. Section IV presents the simulations conducted and results that demonstrate improved performance with our proposed algorithm modifications. Section V presents the hardware, field experiments, and results that validate the system can be used for real shipwreck mapping.

II. BACKGROUND

In recent years, photogrammetry has been used to document and study underwater archaeological sites [1], [2]. The resulting 3D reconstructions are used by archaeologists to study the site and inform the excavation of artifacts. The photogrammetric data needed to create the visualization come from triangulation using still images from the video data [3]. When considering the data needed for photogrammetry, it is important to note that larger variations in camera angle yield more accurate range calculations from triangulation [4].

More recently, AUVs have been used to collect sensor data for photogrammetric reconstruction of marine archaeological sites [5], [6], [7], [8]. Generally, these surveying missions are planned in an ad-hoc manner. In [5], an AUV was used to survey a shipwreck with multiple manually-programmed lawnmower patterns over 30 x 45 m of seafloor. The AUV missions took over 6 hours and much of the mission time was spent surveying parts of the ocean floor that did not contain the shipwreck.

Robotics motion planning is a well-studied field. One standard solution in discrete grid workspaces are exact cell decomposition algorithms such as A*, because they can achieve optimality [9], [10]. However, such a motion planning approach would be computationally intensive when applied to robots with high dimensional configuration spaces, such as AUVs that require minimum 6 DOF states.

To minimize computational complexity in high dimensional spaces, algorithms such as the Rapidly-Exploring Random Tree (RRT) have been developed [11], [12]. RRTs can be used when path planning for robots with dynamic constraints [13], [14]. Both of these features make RRTs ideal for AUV path planning. However, due to their random approach, pure RRT algorithms may not reach optimality.

Modified RRT algorithms, such as RRT*, have been developed to improve planning performance. RRT* achieves asymptotic optimality through a modification in its expansion step[15]. Instead of searching the roadmap for the nearest neighbor, it checks for connections with all neighbors within a certain radius.

Another such modification is RRT-Smart which employs two modifications to the RRT that enable it to converge faster than RRT* [16]. One modification is path optimization, which does a check to shorten the path on each expansion step. Another modification is intelligent sampling, which refers to selectively sampling nodes with a higher likelihood of success.

In [17], an offline motion-planning algorithm specific to photogrammetric reconstruction from an AUV was proposed. The algorithm uses previous data to inform a new path for the AUV that favors areas that have a higher likelihood of containing Objects of Interest. The simulation results of this method show that it favors total coverage of the workspace.

Inspired by these algorithms, the work presented here improves on existing probabilistic motion planning methods for the application of surveying archaeological sites. Details of the motion planning pipeline and field experiment results are described below.

III. AUV ARCHAEOLOGICAL SITE MAPPING METHODOLOGY

In this paper, we propose a multi-mission approach to collecting the image data necessary for photogrammetry of underwater archaeological artifacts. Figure 2 shows a block diagram describing the multiple mission pipeline.

During the first mission, the AUV is equipped with a sonar (either side scan or multibeam sonar) and deployed on a search mission to follow some trajectory T_{search}, e.g. a lawnmower pattern. The sonar data Z_{search} collected during the search mission is then used to create a 3D occupancy grid C of the volume surveyed. From C, an information map is computed that can inform the trajectory planner algorithm's objective function. Both C and I are used by the RRT algorithm to generate a dynamically feasible AUV trajectory $T_{mapping}$ for mapping the site.

The AUV will then be deployed on a second mission to follow $T_{mapping}$ equipped with a camera to collect images $Z_{mapping}$ that can be used to create a 3D photogrammetric reconstruction M of the archaeological site. The map M can be used to create a new information map, new trajectory $T_{mapping}$, and new mission for additional data collection and improved mapping. Each step in this block diagram is described below.

A. Search Trajectory

For the initial AUV mission deployment, a search trajectory aimed to maximize coverage is employed. The search trajectory is manually planned and is typically a lawnmower pattern, e.g. Fig. 3b. During this mission, the AUV collects position and sonar data which is used to generate a coarse occupancy grid that is used for both obstacle avoidance and area of interest (AOI) identification.

B. Occupancy Grid Map Construction

The sonar data from the search trajectory is used to generate an occupancy map C used for obstacle avoidance in motion planning as well as generating the information map I. In this study, a multibeam sonar is used (see the sonar scan plane is shown in Fig. 3a), but the work can be extended to also use a side-scan sonar.

The 3D occupancy grid is represented as $C = \{c_{ijk} | i = 1, ..., m; j = 1, ..., n; k = 1, ...o\}$. The three dimensions of C refer to discretized values of the x, y, and z coordinates of the workspace. Each cell of the occupancy grid has a likelihood of being occupied such that $c_{ijk} \in [0, 1]$. The occupancy grid is initialized such that the known empty cells near the surface have an occupancy of 0.1 and the cells below a certain depth have an occupancy of 0.5. An occupancy of 0.5 implies that the occupancy of that cell is completely unknown.

The cells of the occupancy grid are updated using data collected from the multibeam sonar. The multibeam sonar outputs Z_{search}, a vector of signal strengths for a given bearing ψ, where each signal strength in the vector is associated with a range. Specifically $Z_{search} = \{z_i | i = 1..m\}$ for m different bearing angles and $z_i = [\psi_i \ ss(\psi_i, r_0) \ ss(\psi_i, r_1) \ ... \ ss(\psi_i, r_n)]$ for n range values r_i as illustrated in Figure 3a.

To determine the cell to update for a given z_i, the range and bearings, which are referenced within the sonar's local coordinate frame, must be raycasted to the global coordinate frame. The sonar is mounted to the AUV with some offset yaw, pitch, and roll that can be represented as $[\alpha \ \beta \ \gamma]^{auv}_{son}$ with corresponding rotation matrix R^{auv}_{son}. The AUV has a yaw, pitch, and roll with respect to the global frame: $[\alpha \ \beta \ \gamma]^{G}_{auv}$ with corresponding rotation matrix R^{G}_{auv}. Therefore, the global position of a cell corresponding to a range r and bearing ψ can be found using rigid body transformations:

$$\begin{bmatrix} x_c \\ y_c \\ z_c \end{bmatrix}_G = \begin{bmatrix} x_{auv} \\ y_{auv} \\ z_{auv} \end{bmatrix}_G + R^G_{auv} R^{auv}_{son} \begin{bmatrix} r \cdot cos(\psi) \\ r \cdot sin(\psi) \\ 0 \end{bmatrix} \quad (1)$$

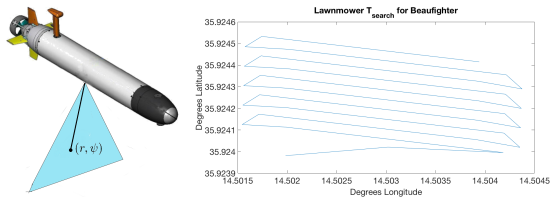

(a) (b)

Fig. 3: The AUV sonar scan plane with a sample (r, ψ) is shown in (a). An example lawnmower trajectory conducted over the Beaufighter plane wreck in St. Julian's Bay, Malta is shown in (b).

For each cell c_{ijk} determined to intersect with a particular ray ψ, r cast by the sonar head, its occupancy is updated using Baye's rule:

$$\begin{aligned} P(c_{ijk,t}) &= P(c_{ijk,t} | ss(\psi, r)_t) \\ &= \frac{P(ss(\psi, r)_t | c_{ijk,t-1}) P(c_{ijk,t-1})}{P(ss(\psi, r)_t)} \end{aligned} \quad (2)$$

In Eq. 2, $P(c_{ijk,t})$ is the probability the cell is occupied, $P(ss(\psi, r)_t)$ is the probability of obtaining signal strength measurement $ss(\psi, r)_t$, and $P(ss(\psi, r) | c_{ijk,t})$ is the probability of obtaining measurement $ss(\psi, r)_t$ given a sonar model and that cell $c_{ijk,t}$ is occuped.

Updating cells in the occupancy grid is accomplished for each sonar measurement obtained during the search mission to produce the final occupancy grid C.

C. Information Map Construction

Once the occupancy grid C has been updated from the search trajectory, it can be used to construct an information map I that can be queried by the motion planner to calculate the information gain associated with potential AUV actions. The goal of this planner is to create a trajectory that leads the AUV over areas of interest, i.e. shipwrecks, from multiple sensor vantage points.

First, a thresholding function is applied to C to create a grid $C_\tau = \{c_{\tau,ijk} | i = 1, ..., m; j = 1, ..., n; k = 1, ...o\}$. Any cell c_{ijk} in C with a likelihood of occupancy above τ_{occ} is considered occupied in the corresponding cell $c_{\tau,ijk}$ of C_τ. For this paper, the threshold is set as $\tau = 0.4$.

The occupancy grid C_τ is then converted to a 2D elevation map matrix, $E = \{e_{ij}], i = 1, ..., m; j = 1, ..., n\}$. In this case e_{ij} is the maximum height (in meters) of all occupied cells in C_τ with horizontal planar coordinate indices i, j. The elevation map of the Bristol Beaufighter plane wreck is shown in Fig. 4a.

In order to find the areas of high elevation variation, the gradient G of the elevation map E is calculated using the Sobel operator.

$$G = \sqrt{G_x^2 + G_y^2} \quad (3)$$

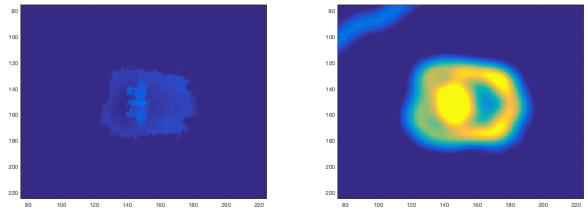

(a) (b)

Fig. 4: (a) An elevation map for the Beaufighter wreck (b) The gradient resulting weighting function after applying the areas of interest detection algorithm.

$$G_x = \begin{bmatrix} -1 & 0 & +1 \\ -2 & 0 & +2 \\ -1 & 0 & +1 \end{bmatrix} * E \tag{4}$$

$$G_y = \begin{bmatrix} -1 & -2 & -1 \\ 0 & 0 & 0 \\ +1 & +2 & +1 \end{bmatrix} * E \tag{5}$$

Since the state estimation of the AUV has an associated error, the position of the elevation map will also be subject to errors. To account for such error, a Gaussian low-pass filter is applied to the gradient map by convolving G with a Gaussian Blur Kernel B. The standard deviation of the Gaussian filter is equal to the uncertainty in state estimation. The equation for the 2D Gaussian Blur is:

$$B(x,y) = \frac{1}{2\pi\sigma^2_{X_{auv}}} e^{-\frac{x^2+y^2}{2\sigma^2_{X_{auv}}}} \tag{6}$$

Finally, the information map, I can be determined by convolving the blur matrix with the gradient matrix.

$$I = B * G \tag{7}$$

The information map will be used to weight the importance of each cell in the objective function used when motion planning. Archaeological sites, such as shipwrecks, have a higher variation in elevation than their surrounding environment, so we propose that areas with a high degree of elevation change should have a higher objective score. The information map for the Bristol Beaufighter site is shown in Fig. 4b.

D. Motion Planning

1) MP Problem Definition: In our problem, we are given a workspace W with physical boundaries and an initial robot configuration X_0 that is located within the boundaries of W. The goal is to determine the time limited sequence of control actions $U = \{u_0, u_1, u_2, ..., u_p\}$ that maximize the information gain. To summarize, our problem is to:

Find

$$\underset{U}{max} O(U, X_0) \tag{8}$$

Subject to

$$O(U, X_0) = \sum_{X_D \in E} Info(I, X_D) \tag{9}$$

$$E(U, X_0) = \bigcup_{l=0}^{p} X_{l,D} \tag{10}$$

$$X_{l,D} = D(X_l) \tag{11}$$

$$X_{l+1} = f(u_l, X_l) \tag{12}$$

In the above optimization problem, the function $f(u_l, X_l)$ returns AUV state X_{l+1} after it applied control effort u_l from the previous state X_l.

The function $D(X_l)$ returns $X_{l,D}$, a discretized version the AUV state vector X_l. In this case, the first 3 elements of $X_{l,D}$ are the integer index values associated with the closest 3D cell of C, and the last element corresponds with an integer index value associated with a discretization of the AUV's yaw angle. E.g., if the state X_l is contained within cell $c_{3,4,6}$ of C, and the yaw angle is 85 degrees, then the discretized state is $X_{l,D}$ = [3 4 6 1] for and angle discretization resolution of 90 degrees.

The set $E(U, X_0)$ of Eq.10 refers to the union of all discritized states visited over the course of a trajectory that follows the p control actions of the set U. Finally, the function $Info(I, X_D)$ returns the information gain when the AUV resides at the discritized state X_D of the information map I.

2) MP Algorithm: The purpose of this algorithm is to generate trajectories for the AUV to optimize data collection for photogrammetry. The trajectories are generated using a RRT that maximizes the above described scoring function. Our modified RRT is described in Algorithm 1. Several key modifications to the RRT structure are described below.

3) Node Selection for Expansion: Line 3 of Alg. 1 calls the $selectNodeToExpand$ function. In the general RRT implementation, a random configuration from the space is sampled and the closest node in the tree is selected for expansion. In the implementation presented in this paper, nodes are selected using two different sampling methods. A parameter γ is used to select the frequency at which these two methods are used.

The first method aims to generate a distribution paths in the RRT with path duration uniformity. To accomplish

Algorithm 1 Modified RRT

1: Add start configuration c_{start} to $R(N, E)$
2: **for** $i \leftarrow 1$ **to** $numcycles$ **do**
3: $c \leftarrow$ selectNodeToExpand($R(N, E)$)
4: $c' \leftarrow$ expandNewNode(c)
5: **if** edge e from c to c' is collision-free **then**
6: $prune(c, c')$
7: compute score of c
8: Add (c, e) to R
9: **if** c' in endgame region **then**
10: path
11: **end if**
12: **end if**
13: **end for**
14: **return** path with best score

Algorithm 2 Expansion Step

$p \leftarrow parent$
$depth \leftarrow rand()(maxDepth - minDepth) + minDepth$
$diveDist \leftarrow dynamicDive(depth)$
$surfDist \leftarrow rand()(maxSurfDist - minSurfDist) + minSurfDist$
if $rand() > \gamma$ **then**
  $h = HICs(rand() \cdot numHICs)$
  $\theta \leftarrow atan2(h.Pose(y) - p.Pose(y), h.Pose(x) - p.Pose(x))$
else
  $\theta = rand() \cdot 2\pi$
end if
$circlePose.x = R * (cos(p.yaw) + cos(p.yaw + \theta))$
$circlePose.y = R * (sin(p.yaw) + sin(p.yaw + \theta))$

this, the node selection first randomly selects a time no greater than the maximum mission time. The node with the timestamp closest to the random time is selected for expansion. This ensures the RRT will generate paths of varying duration.

The second method to node selection for expansion is to only select from the nodes considered to be a High Information Configuration (HIC). This method encourages the RRT to expand in areas where there is high information gain.

4) Expansion to New Nodes: Line 4 of Alg. 1 calls the $expandNewNode$ function, which is provided in Alg. 2. To account for AUV dynamics and constraints in localization, the RRT expansions must have two characteristics. First, the edge should incorporate a straight segment, in which the flyover occurs just above the site of interest. This provides a stable path for accurate Doppler Velocity Log (DVL) based dead-reckoning localization. Second, the edge should include a surfacing before and after the flyover to obtain GPS measurements, again to increase accuracy in vehicle localization.

To accomplish the two goals, the random node expansions in this algorithm use a series of steps, (see Fig. 5a and 5b). The first step is an arc of random length, where the radius of the arc is the minimum turn radius of the vehicle. Hence the first step of the expansion is used to incorporate a random change in the yaw direction. This change in yaw occurs at the surface.

Next, the AUV drives straight for a distance to increase velocity, then dives to its desired depth, holds the depth for a random distance, and returns to the surface. The expansion step of the RRT algorithm is illustrated in Fig. 5a, Fig. 5b and described in Alg. 2.

The direction of expansion of the RRT, θ is selected in one of two ways. A portion of the time, the angle is selected randomly. The rest of the time, the RRT expands towards a randomly selected HIC or a node with a relatively high score. The variable γ denotes the probability of a random

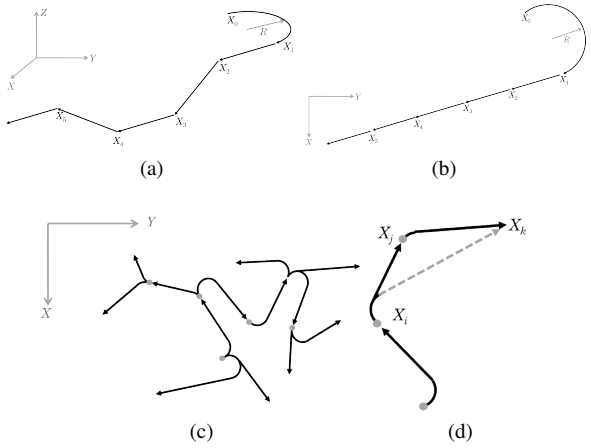

Fig. 5: Node Expansions: In (a), a 3D visual of a single multi-step node expansion is shown. In (b), a top down view of the same expansion can be seen. Multiple expansions in a RRT are shown in (c).The pruning step (d) of the RRT creates a shorter path from the grandparent to end of the new node. The dotted line represents a potential pruning step.

expansion versus an expansion towards a HIC.

Once a node is generated, the objective function is calculated for the node. If the score of the node is higher than a threshold, that node is added to a list of "HICs", $H \subseteq N$. These HICs can help the RRT expand in regions with more AOI.

5) Edge Pruning: Another proposed modification to the algorithm is the addition of a pruning step (illustrated in Figure 5d). With each expansion from a parent, the score of the edge connecting the parent to the new node is compared to the score of an edge from the grandparent to the new node. If the pruned objective score is higher, the parent node and its edges will be removed. More specifically, an edge will be pruned if $\frac{O(E_{ik})}{t_{ik}} > \frac{O(E_{ij} + Ejk)}{t_i j + t_i k}$.

The edge from the grandparent to the new node has the same steps as the expansion stage. The depth is chosen to be the same as the edge from the parent to new node and the rest of the components are calculated to satisfy the path length and dynamic constraints of the AUV.

6) Objective Function: RRTs are traditionally used to efficiently find a collision-free trajectory in a complex environment. For this study, the goal of the RRT is to maximize information gain given time constraints. The information gain is quantified by the score function defined by Equation 9.

7) Endgame Region: Commonly, the endgame region of an RRT is defined as within a threshold of a goal pose for the robot. In this case, the robot is not navigating to an end goal, but creating a path to maximize information gain within a maximum duration of time. Therefore, the endgame region is defined as any path longer than the minimum path length is in the endgame region.

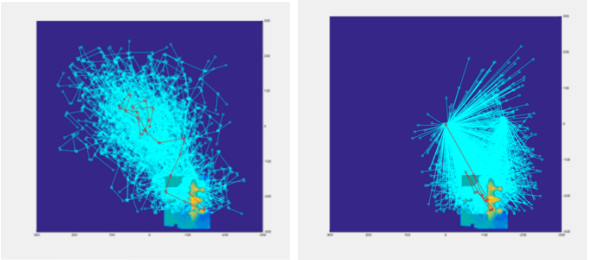

(a) (b)

Fig. 6: (a) Shows a roadmap for an expansion without HICs. (b) for an expansion step using HICs. Note the efficiency and multiple flythroughs over the wreck in (b).

E. 3D Mapping

After the AUV is deployed to track the trajectory $T_{mapping}$ constructed by the RRT, the recorded video data can be processed to produce a 3D map. Stills are grabbed from the video footage and processed using off-the-shelf software, specifically Agisoft Photoscan. The output of Agisoft photoscan is a 3D rendering that is the end product of this archaeological site mapping pipeline. Outputs of Agisoft Photoscan are shown in Figures 8b and 8d.

IV. SIMULATIONS

A. Simulation Setup

The archaeological site motion planner was implemented in MATLAB. A series of simulations were conducted to evaluate the effectiveness of the RRT algorithm and modifications. These simulations were conducted using data collected from archaeological sites. The data used to create the occupancy grid and information map for the Beaufighter wreck comes from data collected prior to this study. The simulations were used to observe differences in roadmap generation as well as the score of the best path.

The metric used to evaluate the algorithms is the above mentioned score function. Due to their random nature, RRTs tend to perform better with more expansion steps. To characterize the performance of the algorithm, the best path score is calculated for a range of $numcycles$.

B. Simulation Results

The HIC node selection shows noticeable qualitative results. Figures 6a and 6b show the results of a roadmap generated without the use of HICs and with the use of HICs, respectively. The information map used shows the Beaufighter wreck located in the bottom-right corner of the map. While Figure 6a indicates a high coverage of the workspace, Figure 6b shows a preference of the RRT algorithm to expand towards an area of interest. The final RRT (in red), shows multiple passes over the AOI.

The RRT modifications are further evaluated with respect to the scoring function. The RRT performance as a function of number of trials was computed for: the original RRT algorithm, RRT with pruning, RRT with HICs, and RRT with both pruning and HICs. The results are shown in Figure 7a. All four methods lead to an asymptotic score of approximately 1200 which is likely due to the maximum score given time limitations on the motion plan. The results indicate that pruning generally causes the RRT to reach the asymptote slightly faster. The use of HICs for expansion causes the RRT to reach the asymptote at approximately 700 cycles. Both HICs and pruning do not improve the performance of the algorithm.

The score improvement of the RRT modifications is shown in Figure 7b. The HIC modification has a maximum score improvement of 152% over the original RRT algorithm at 500 cycles. The pruning modification has a maximum score improvement of 102% over the original algorithm at 700 cycles. Both of these modifications indicate that the modifications improve the performance of this RRT implementation.

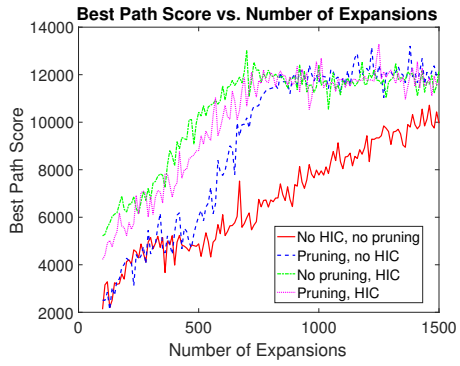

(a)

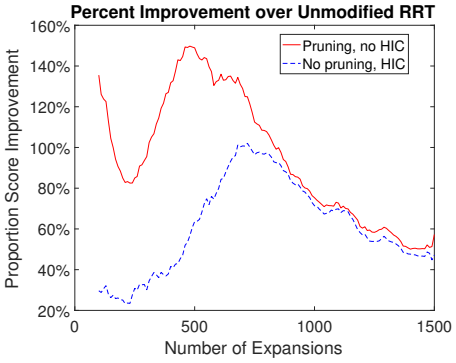

(b)

Fig. 7: (a) shows the score of the best path given a number of cycles for the different RRT modifications. (b) shows the score improvement of the RRT modifications.

V. EXPERIMENTS

A. Hardware

The AUV used in this study is an Iver2 purchased from OceanServer. It is driven by a propeller, and four actuated fins control roll, pitch, and yaw of the robot. Its sensors include a 3DOF compass, altimeter, DVL, and GPS receiver. A BlueView M900-2250 Dual Frequency Series sonar was also mounted to the AUV for data collection in this study.

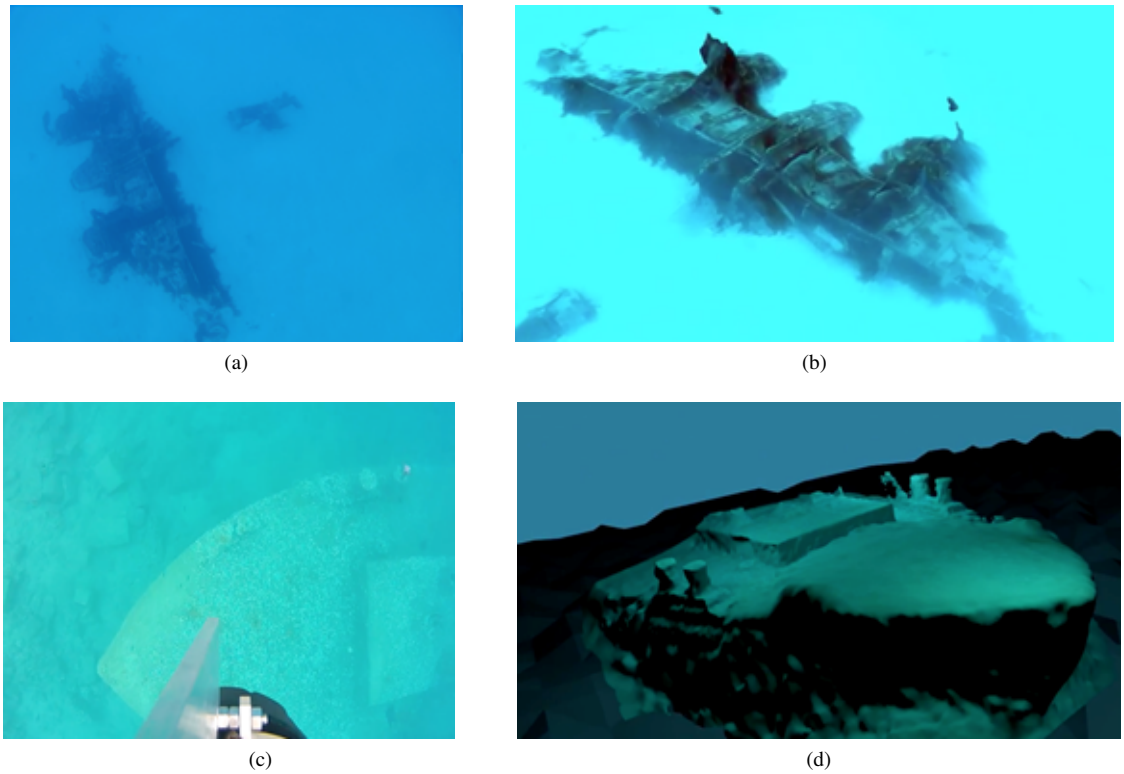

(a) (b) (c) (d)

Fig. 8: (a) An image of the Beaufighter wreck taken by a GoPro on the AUV. (b) A reconstruction of the Beaufighter wreck from a lawnmower pattern mission. (c) An image of the X-Lighter taken from the AUV. (d) A reconstruction of the X-Lighter wreck from two RRT missions

Date	Location	Trajectory Type	Mission Time	Reconstruction Use
06/01	Big Fisherman's Cove	Manual Search	20m	Catalina Information Map
06/15	Manoel Island	Manual Search	6m	Manoel Information Map
06/23	St. Julian's Bay	Lawnmower	56m	Beaufighter
06/27	Manoel Island	RRT Mapping	8m	Bow of X-Lighter
06/28	Manoel Island	RRT Mapping	9m	Midsection of X-Lighter

TABLE I: List of deployments of the AUV to collect data for use with the archaeological site pipeline.

For collection of video data, a variety of GoPros were used from versions HERO1, HERO2, and HERO3. The AUV can be driven manually and wirelessly on the surface or be programmed for waypoint navigation.

B. Field Experiments Setup

A series of field experiments were conducted to verify the feasibility of the archaeological mapping pipeline. A comprehensive list of the missions used for the data collection for this paper are presented in Table I.

The first set of experiments were to test the search trajectory and the information map generation. These trials were conducted at Big Fisherman's Cove, Catalina Island, CA and at Manoel Island, Malta. The trials conducted in Catalina were used to validate the manual search trajectory and information map generation portion of the pipeline. The focus of these missions were a small boat wreck in the cove. The trials conducted at the southern end of Manoel Island near the X-Lighter Coralita shipwreck were used to create an information map for a real archaeological site.

The second set of experiments were used to collect data for archaeological site reconstruction. These experiments were conducted at Manoel Island, Malta and at St. Julian's Bay. The mapping missions included a combination of lawnmower missions and RRT missions.

C. Field Experiment Results

The data collected from the search trajectory missions in Catalina and Malta were successfully used to create Information Maps of the respective areas. The Information Map for the Beaufighter wreck was generated using data collected prior to this study. The RRT missions planned using the previously described algorithm were successfully executed by the AUV. The field deployments validate the feasibility of the generated paths. The data collected from the mapping missions were successfully used to create photogrammetric reconstructions of the archaeological sites. Examples of image data collected from the Beaufighter and X-Lighter sites are shown in Figure 8a and Figure

8c respectively. Figure 8b shows a reconstruction of the Beaufighter site from data collected with lawnmower missions. Figure 8d shows a reconstruction of the X-Lighter Coralita site using data collected with RRT missions. All reconstructions were generated using Agisoft Photoscan.

VI. CONCLUSIONS & FUTURE WORK

The results of this study present a novel method of using AUVs to survey archaeological sites. The data collection begins with a search trajectory which is used a create a coarse sonar map of this area. This sonar map is used to generate an information map which highlights areas of interest. The information map and sonar occupancy grid are used to inform a modified RRT motion planning algorithm. The expansion step of the RRT algorithm was modified to prune low information edges and grow towards High Information Configurations. The modifications to the RRT algorithm have been shown to increase objective scores by up to 152% when compared with the original RRT algorithm in simulation. Furthermore, the full marine archaeological site mapping pipeline has been validated in field trials that have resulted in 3D reconstructions of two archaeological sites off the coast of Malta.

Future work could expand on this work to use different sensors for the search and mapping trajectories. Specifically, the area of interest map could be generated using a side-scan sonar. Furthermore, the archaeological site photogrammetric reconstruction could fuse sonar data with the photo data to create more accurate representations. Finally, we could extend the pipeline to a multi-robot system.

ACKNOWLEDGMENT

This material is based upon work supported by the National Science Foundation under Grant No. 1460153. This work was performed in part at the Claremont Colleges Robert J. Bernard Biological Field Station and at the University of Southern California Wrigley Marine Science Center. We also thank Apoorva Sharma for his initial work on mapping.

REFERENCES

[1] P. Drap, D. Merad, B. Hijazi, L. Gaoua, M. M. Nawaf, M. Saccone, B. Chemisky, J. Seinturier, J.-C. Sourisseau, T. Gambin, and F. Castro, "Underwater photogrammetry and object modeling: A case study of xlendi wreck in malta," *Sensors*, vol. 15, no. 12, pp. 30 351–30 384, 2015.

[2] T. Gambin, "A phoenician shipwreck off gozo, malta," *The Journal of the Archaeological Society, Malta*, 2011.

[3] G. Olague and R. Mohr, "Optimal camera placement for accurate reconstruction," *Pattern Recognition*, vol. 35, no. 4, pp. 927 – 944, 2002.

[4] M. Bern, D. Eppstein, and J. Gilbert, "Provably good mesh generation," *J. Comput. Syst. Sci.*, vol. 48, no. 3, Jun. 1994.

[5] B. Bingham, B. Foley, H. Singh, R. Camilli, K. Delaporta, R. Eustice, A. Mallios, D. Mindell, C. Roman, and D. Sakellariou, "Robotic tools for deep water archaeology: Surveying an ancient shipwreck with an autonomous underwater vehicle," *Journal of Field Robotics*, vol. 27, no. 6, pp. 702–717, 2010.

[6] P. Ozog, G. Troni, M. Kaess, R. Eustice, and M. Johnson-Roberson, "Building 3d mosaics from an autonomous underwater vehicle and 2d imaging sonar," in *IEEE International Conference on Robotics and Automation*, 2015, pp. 1–8.

[7] K. Skinner and M. Johnson-Roberson, "Detection and segmentation of underwater archaeological sites surveyed with stereo-vision platforms," in *MTS/IEEE OCEANS*, 2015.

[8] S. Seibert von Fock, S. Bilich, K. Davis, V. K. Viswanathan, Z. Lobo, J. Lupanow, C. Clark, T. Gambin, and W. Z., "Pipeline for reconstruction and visualization of underwater archaeology sites using photogrammetry," in *32nd International Conference on Computers and Their Applications*, 2017.

[9] H. Choset, "Coverage for robotics - a survey of recent results," *A. of Mathematics and Artificial Intelligence*, vol. 31, pp. 113 – 126, 2001.

[10] J. Canny and J. Reif, "New lower bound techniques for robot motion planning problems," in *28th Annual Symposium on Foundations of Computer Science (sfcs 1987)*, Oct 1987, pp. 49–60.

[11] J. Kim and J. P. Ostrowski, "Motion planning a aerial robot using rapidly-exploring random trees with dynamic constraints," in *2003 IEEE International Conference on Robotics and Automation*, vol. 2, Sept 2003, pp. 2200–2205.

[12] J. Poppinga, A. Birk, K. Pathak, and N. Vaskevicius, "Fast 6-dof path planning for autonomous underwater vehicles (auv) based on 3d plane mapping," in *2011 IEEE International Symposium on Safety, Security, and Rescue Robotics*, Nov 2011, pp. 345–350.

[13] S. M. Lavalle, "Rapidly-exploring random trees: A new tool for path planning," Tech. Rep., 1998.

[14] S. M. Lavalle, J. J. Kuffner, and Jr., "Rapidly-exploring random trees: Progress and prospects," in *Algorithmic and Computational Robotics: New Directions*, 2000, pp. 293–308.

[15] S. Karaman and E. Frazzoli, "Sampling-based algorithms for optimal motion planning," *CoRR*, 2011.

[16] F. Islam, J. Nasir, U. Malik, Y. Ayaz, and O. Hasan, "Rrt *-smart: Rapid convergence implementation of rrt * towards optimal solution," in *2012 IEEE International Conference on Mechatronics and Automation*, Aug 2012, pp. 1651–1656.

[17] M. Candeloro, F. Mosciaro, A. J. Srensen, G. Ippoliti, and M. Ludvigsen, "Sensor-based autonomous path-planner for sea-bottom exploration and mosaicking," *IFAC*, vol. 48, no. 16, pp. 31 – 36, 2015, 10th {IFAC} Conference on Manoeuvring and Control of Marine Craft.